J Nanopart Res (2019) 21: 53
https://doi.org/10.1007/s11051-019-4488-3

RESEARCH PAPER

Nanostructured Zn-Ti layered double hydroxides with reduced photocatalytic activity for sunscreen application

Orielia Pria Egambaram · Sreejarani Kesavan Pillai · Marlize Lategan · Suprakas Sinha Ray

Received: 10 September 2018 / Accepted: 14 February 2019 / Published online: 9 March 2019

Abstract The harmful effects of long-term UV exposure on human skin are increasingly understood these days, and therefore, the use of topical sunscreen products containing UV filters has significantly increased. Although the currently used organic and inorganic UV filters are effective UV absorbers, they may cause several problems such as high photoreactivity, photodegradation, and generation of reactive oxygen species leading to serious skin damages including skin cancer. Therefore, the development of safer, skin-compatible, photostable, and more effective photoactive ingredients is critical. In this study, a Zn-Ti layered double hydroxide (Zn-Ti LDH) was prepared using a hydrothermal method, and its properties as a sunscreen additive were evaluated and compared to those of nano-TiO_2 and nano-ZnO. Physical characterization confirmed the formation of a highly stable crystalline LDH structure. Scanning electron microscopy analysis revealed the formation of two-dimensional nano-flakes and layered structure. The optical properties of Zn-Ti LDH analyzed by diffuse reflectance UV-Vis showed higher UV reflection properties and lower absorption properties in comparison to TiO_2 and ZnO. Zn-Ti LDH exhibited substantially lower levels of photocatalytic activity towards the degradation of methylene blue at both 365 nm and 254 nm which indicates increased safety of Zn-Ti LDHs for use as UV filters in topical sunscreen applications.

Keywords Zn-Ti LDH · Synthesis · Characterization · Optical and photochemical properties · Nanostructured catalysts

O. P. Egambaram · S. K. Pillai (✉) · S. S. Ray
DST/CSIR National Centre for Nanostructured Materials, Council for Scientific and Industrial Research, Pretoria 0001, South Africa
e-mail: skpillai@csir.co.za

O. P. Egambaram · S. S. Ray
Department of Applied Chemistry, University of Johannesburg, Doornfontein, Johannesburg 2028, South Africa

M. Lategan
Photobiology Laboratory, Sefako Magkatho Health Science University, Molotlegi Street, Ga-Rankuwa, Pretoria, South Africa

Introduction

Premature skin aging, skin cancer, burning, erythema, and pruritus are some of the major environmental stress agents for human skin which are caused by ultraviolet radiation (UVR) and have resulted in the widespread use of sunscreen agents (Perioli et al. 2006). However, the efficacy, as well as the safety of the sunscreen agents, especially the organic UV filters which they contain, has been brought into question lately. Organic UV filters are typically chemical compounds that absorb UVR and release it as heat or energy which can evoke photoallergic reactions on the skin. Due to their relatively low molecular weight and lipophilic character, most of the organic UV filters are able to cross the skin barrier. Certain allergic reactions or toxic degradation products may arise as sunlight transforms these UV filters into reactive intermediates which may penetrate deeper causing further stress to the skin (Perioli et al.

2006). Due to such properties, they are more likely to cause skin toxicity making inorganic UV filters preferable for the use in sunscreen formulations (Manaia et al. 2013; Fajzulin et al. 2015).

Inorganic filters have several advantages over organic UV filters; they offer broad-spectrum UV protection in both the UVA (320–400 nm) and UVB (290–320 nm) regions and they are known to be structurally more stable than their organic counterparts (Manaia et al. 2013). The attenuation of UVR in this case is due to scattering and reflection instead of absorption. Nanoparticles of ZnO and TiO_2 have been commonly used as inorganic UV reflectors in various sunscreen products. ZnO typically provides protection within the UVA range whereas TiO_2 covers UVB and part of UVA (Manaia et al. 2013). The increased use of inorganic UV filters has been mainly due to their cosmetic efficacy and their decreased likelihood to produce irritant reactions (Serpone et al. 2007). However, TiO_2 and ZnO nanoparticles tend to agglomerate in the formulation and numerous studies have shown that this affects their UV reflection and absorption properties. Furthermore, it is often forgotten that despite their good UV-shielding properties, ZnO and TiO_2 are known photocatalysts and their high photoreactivity could be a serious concern when considering the skin safety of the consumer. The main issues such as genotoxicity and cytotoxicity of photocatalysts are linked to their photocatalytic properties (Smijs and Pavel 2011). Therefore, it is crucial to develop effective UV-shielding materials with lower photoreactivity, good structural stability, and high UV reflection/scattering properties.

LDHs are either synthetic or naturally occurring materials which are comprised of inorganic elements and have a two-dimensional structure similar to that of brucite with formula ($M^{II}(OH)_2$). The general formula for LDHs is $[M^{II}_{1-x}M^{III}_x(OH)_2]^{x+}\cdot[(A^{n-}_{x/n})\cdot mH_2O]^{x-}$, where M^{II} and M^{III} and A^{n-} represent the divalent, trivalent cations and interlayer anion group, respectively. The presence of the metal cations gives an overall positive charge to the layers within the structure which is compensated by either the interlayer anion or water molecules between the layers (Xu and Braterman 2010; Seftel et al. 2015).

Work by Shao et al. (2011) reported that Zn-Ti LDHs have higher photocatalytic activity than ZnO and TiO_2. However, a recent study by Li et al. (2017) highlighted the possibility of using Zn-Ti-CO_3-LDH as a UV attenuator; nevertheless, no study was done towards measuring the photocatalytic activity towards sunscreen application. The mechanism of UV shielding was reported due to the absorption rather than the reflection of UVR. However, the results presented in this paper contradicted the proposed interpretation thereof (Li et al. 2017).

Within the field of photoprotection, investigations have been conducted regarding the intercalation of *p*-aminobenzoic acid (PABA) within two kinds of LDHs (Mg-Al and Zn-Al LDH). In this study, LDHs were used to protect the organic UV filters from degradation and this provided further photostability for the molecules (Perioli et al. 2006). Furthermore, Cursino et al. (2013) focused on the intercalation of a Zn-Al LDH with benzophenone in the presence of anionic surfactants and its use as a sunscreen material. Their study revealed good adsorption for UVA, UVB, and UVC range owing to the enhanced photostability of benzophenone offered by LDH layers. Despite the research conducted on the intercalation of anionic surfactants and active ingredients into LDHs for photoprotection, the use of unmodified LDHs as an ingredient for sunscreen application is seldom.

Hence, the focus of this work was to develop a structurally and photochemically stable two-dimensional nanostructured Zn-Ti LDH as safer and more efficient UV protective agent for topical applications. It was envisaged that the combination of Zn and Ti in a two-dimensional structure is an effective way to alter the band gap and to reduce the photocatalytic activity. The synergistic effect of Ti and Zn in the same crystalline structure is expected to increase the degree of UV scattering of the material and hence the UV protection efficiency. The hydrophilicity, swelling capacity, and white color of the material also are advantageous in terms of stabilization, rheological modification, and esthetics of cosmetic formulations.

Experimental methodology

Materials and chemicals

Zinc nitrate hexahydrate (98%, Sigma-Aldrich), titanium isopropoxide (99.999%, Sigma-Aldrich), urea (99.8% supplied by AMKA), and sodium hydroxide (98%, Merck) were purchased from various suppliers and were used without further purification. Cosmetic grade nano-ZnO and nano-TiO_2 kindly supplied by AMKA Pty Ltd., South Africa, were used as references.

Synthesis method

Titanium isopropoxide (0.001 mol), zinc nitrate hexahydrate (0.004 mol), and urea (0.05 mol) were dissolved in deionized water (100 ml) and stirred vigorously at 120 °C for 24 h. Thereafter, the solution was aged at room temperature for 24 h, centrifuged at 4000 rpm for 6 min, and rinsed with distilled water six times. The precipitate was finally rinsed with acetone and dried in the vacuum oven at 120 °C.

Physical characterization techniques

Powder XRD was carried out on the samples as the first round of characterization to provide information regarding the crystallography of the LDH structure. This was done using PANalytical X'Pert PRO, with a Cu Kα source ($\lambda = 0.154$ nm). The surface morphology of the LDH material was studied using scanning electron microscopy using Zeiss Auriga Cobra Focused-Ion Beam FESEM. FTIR of the prepared samples was performed using a Perkin Elmer Spectrum 100 FTIR spectrometer with MIRacle ATR attachment and a Zn/Se plate. A small amount of sample was pressed onto the Zn/Se plate and spectra over the range of 550 to 4000 cm^{-1} at a resolution of 4 cm^{-1}. BET analysis was conducted to determine the specific surface area of the Zn-Ti LDH using a Micrometrics TRISTAR 3000 instrument. The samples were degassed for 2 h prior to the analysis to remove any adsorbed surface contaminants. XPS analysis was used to determine the surface chemical composition of Zn-Ti LDH and also to determine the oxidation state of Ti. A Thermo ESCAlab 250Xi instrument with spot size 900 μm and monochromatic Al kα (1486.7 eV) was used. The pass energy for the high-resolution XPS scans and XPS survey was 20 eV and 100 eV respectively.

Optical and photochemical properties of Zn-Ti LDH

To measure the photoreflectance capabilities of the samples, diffuse reflectance ultraviolet-visible (DRUV-Vis) spectroscopy was employed. DR spectra between 200 and 800 nm were collected using Perkin Elmer Lambda 950 UV-Vis spectrometer equipped with a 150-mm InGeAS integrated sphere at a wavelength resolution of 1 mm. The data obtained from the DRUV-Vis was further used to obtain Kubelka-Munk plot for each of the samples, providing information about their absorption of UVR and bandgap.

Adsorption studies were conducted using methylene blue (MB) to measure the inherent surface interaction of samples with MB in the absence of UVR. Typically, 2 mg of each sample was dispersed in 25 ml of 5 ppm MB solution. The solution was stirred in the dark for 30 min to reach adsorption/desorption equilibrium and the absorbance was measured, using UV-Vis spectroscopy (Perkin Elmer 750 s UV-Vis spectrometer at $\lambda_{max} = 664$ nm). The solutions were stirred for a further 3.5 h in the dark and the absorbance was measured again. The MB adsorption on the surface of the material was calculated according to the following equation:

$$q_e = \frac{\nu}{M}(C_0 - C) \quad (1)$$

where v is the volume of the solution in milliliters, M is the weight of the sample in milligrams, C_0 is the concentration (mg/ml) of the MB solution at 0 h, and C is the concentration (mg/ml) of the solution after 3.5 h (N et al. 2015).

The photocatalytic activity of the samples was analyzed using photodegradation of MB under the irradiation of UV light in UVB and UVA regions ($\lambda = 254$ nm and 365 nm). The UV source was a 6W UV GL-58 handheld UV lamp with a 254 or 365 nm wavelength pass filter. Typically, 6 mg of sample was dispersed in 75 ml of 5 ppm MB solution affording a final solution with a concentration of 0.08 mg/ml. UV-Vis analysis was conducted on each sample prior to UVR to determine the MB concentration before UV exposure. The mixture was stirred in the dark for 30 min to reach adsorption/desorption equilibrium; thereafter, the solutions were stirred for 4 h under UVR (either 365 nm or 254 nm). At specific time intervals, a 3 ml aliquot of solution was removed from each beaker, and this was replaced by 3 ml distilled water. The filtrate was then analyzed using Perkin Elmer 750 s UV-Vis spectrometer at $\lambda_{max} = 664$ nm to find the concentration MB left in the filtrate after UV exposure.

Determination of sun protection factor of Zn-Al LDH

Preliminary in vitro sun protection factor (SPF) evaluation of the Zn-Ti LDH was carried out by using 0.5 g Zn-Ti LDH which was made into a paste and applied between two UV transparent quartz plates. Diffuse reflectance UV transmittance spectra were recorded by a

Perkin Elmer Lambda 950 UV-Vis spectrometer with a 150 mm InGeAS integrated sphere, between 200 and 800 nm, and the spectra were collected at a wavelength resolution of 5 nm. The SPF of Zn-Ti LDH was calculated using Mansur's Equation (Mansur et al. 1986)

$$\mathrm{SPF} = \mathrm{CF} \times \sum_{290}^{320} \mathrm{EE}(\lambda) \times I(\lambda) \times \mathrm{Abs}(\lambda) \qquad (2)$$

where EE is the erythemal effect spectrum at wavelength λ, I is the solar intensity spectrum, Abs. (λ) is the absorbance, and CF is the correction factor 10. The value of EE × I may be taken as constants (refer to Table 3).

Results and discussion

Physical characterization of Zn-Ti LDH

XRD powder diffraction was carried out to determine the formation of the LDH structure as well as to provide information regarding the crystallinity for Zn-Ti LDH and the pattern obtained is given in Fig. 1. A strong (003) basal reflection and weaker (110) reflection was observed, and both peaks are the characteristic of LDH materials. This (003) peak has been previously reported at $2\theta \approx 11.7°$ with a d-spacing of 0.76 nm for LDHs which contained divalent and trivalent cations; however, in this case, the (003) basal reflection was shifted to $2\theta \approx 12.9°$ (Seftel et al. 2008; Shao et al. 2011). The shift to higher 2θ values is indicative of the incorporation of Ti^{4+} in the LDH structure (Shao et al. 2011). Other non-basal reflections which are the characteristic for LDHs are the following: (100), (101), and (113). Their positions may differ depending on the cations present within the LDH structure (Xu and Braterman 2010).

A decrease in the d-spacing is also observed which may be attributed to the strong electrostatic forces which now exist between the host layer and the guest carbonate ions located in the interlayer spaces due to the incorporation of Ti^{4+} (Shao et al. 2011). This finding was further supported by Garcia et al. (Silva et al. 2009) who observed an obvious shift towards a higher 2θ angle in Zn-Ti LDH and according to this source, it is due to the incorporation of Ti^{4+} in the structure. Peaks observed at $2\theta \approx 32°$ and 35.7° correlate to $Zn(OH)_2$ as confirmed by PDF card 00-020-1437 (Shao et al. 2011). A minor peak at $2\theta = 30.75°$ was also observed and this corresponds to rutile TiO_2 (PDF card 00-089-4202) (Shao et al. 2011; Tshabalala et al. 2017a).

XPS provided information about the oxidation states of materials present, namely titanium. Figure 2a shows the full XPS survey for the Zn-Ti LDH. The survey indicated that the surface contained mainly titanium, zinc, carbon, and oxygen. No other elements were observed as impurities on the surface. The Ti 2p spectrum (Fig. 2b) was as expected with two peaks located at 458.3 eV and 464 eV. The two peaks observed correlate to the Ti $2p_{3/2}$ and $2p_{1/2}$ interstitials, respectively (Tshabalala et al. 2017b). The peak at 458.3 eV was deconvoluted into two peaks which were centered at 458.31 eV and 458.65 eV. These correspond to Ti^{4+} interstitials without any trace of Ti^{3+} in the sample. The peaks present indicated the presence of Ti^{4+} in the sample and are in accordance with reports in literature (Shao et al. 2011; Tshabalala et al. 2017a, b). XPS analysis is thus in line with the XRD results and suggests that the surface of the materials synthesized contains only Ti^{4+}.

The elementary XPS analysis showed that the surface atomic percentages of Zn and Ti as 22% and 2.5% respectively. The concentration of Ti at the LDH surface was found to be lower compared to that of Zn indicating its integration within the crystal structure causing fewer Ti remaining on the surface. According to the literature (Seftel et al. 2008), the incorporation of Ti in the crystal structure might reduce its photocatalytic efficiency which is true in this case as could be seen from the photochemical property measurement results.

From the SEM micrograph (Fig. 3), the flake-like morphology characteristic of LDHs was evident. Although it was difficult to confirm the uniformity of this morphology, this SEM micrograph gave an indication that the sample possesses major portion of larger flakes. The observed morphology is in accordance with reports in literature by Shao et al. (2011). TEM analysis of the sample (Fig. 3 insert) verified the formation of platelet/flake-like morphology of Zn-Ti LDH. The micrograph showed well-ordered two-dimensional layered crystalline structure of LDH with varying particle sizes and thicknesses. The particle thickness is estimated to be in the range 20–70 nm approximately.

Figure 4 shows the FTIR spectrum for the Zn-Ti LDH and it clearly indicates the presence of a broad band at 3295 cm^{-1} due to the OH stretching mode of the interlayer water molecules and the hydroxyl groups. The broadness of the OH band may be due to the presence of hydrogen bonds which exist between the various metal

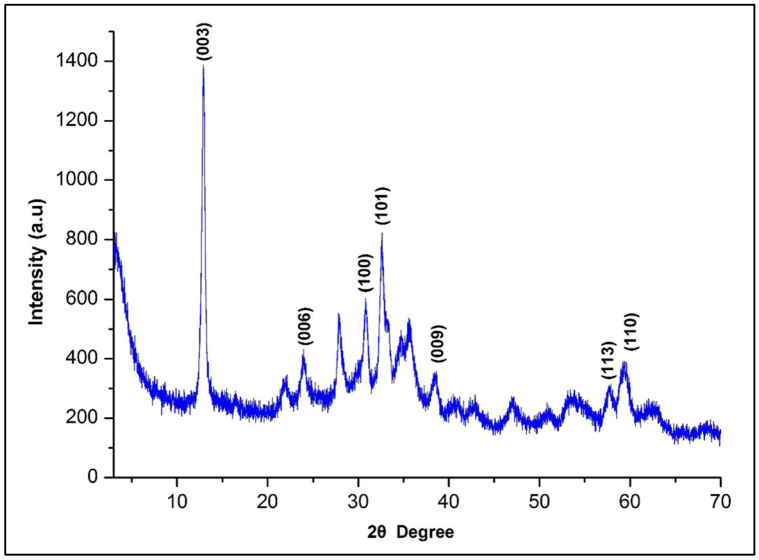

Fig. 1 Powder XRD pattern for Zn-Ti LDH

cations and the OH. The slight shift that is observed is due to the difference in oxidation state between the cations which subsequently affects the strength of the electrostatic forces which exist internally. The electronegativity of these cations affects the electron density on the M-OH bond (Saber and Tagaya 2003). Strong, narrow bands were observed at approximately 1502 cm^{-1} and 1388 cm^{-1} are due to the v_3 bending mode of the interlayer carbonate ions. Weaker bands at 1048 cm^{-1} and 702 cm^{-1} correlate to the v_1 mode of carbonate and free carbonate ions respectively while the two medium bands at 952 cm^{-1} and 837 cm^{-1} are due to the v_2 vibration mode of the carbonates (Saber and Tagaya 2003; Ahmed et al. 2012a). This spectrum thus confirms the presence of carbonate anions within the LDH structure.

The specific areas of the samples were determined using Brunauer-Emmett-Teller (BET) method and a high specific surface area of 77.0 m^2/g was observed for Zn-Ti LDH while the references ZnO and TiO_2 exhibited much lower specific surface areas of 3.2 m^2/g and 8.5 m^2/g, respectively.

Optical and photochemical characterization of Zn-Ti LDH

Diffuse reflectance and band gap determination

Figure 5 shows the DRUV-Vis spectra for Zn-Ti LDH and the two reference samples. The UV reflectance capability of the samples seems to differ and this is

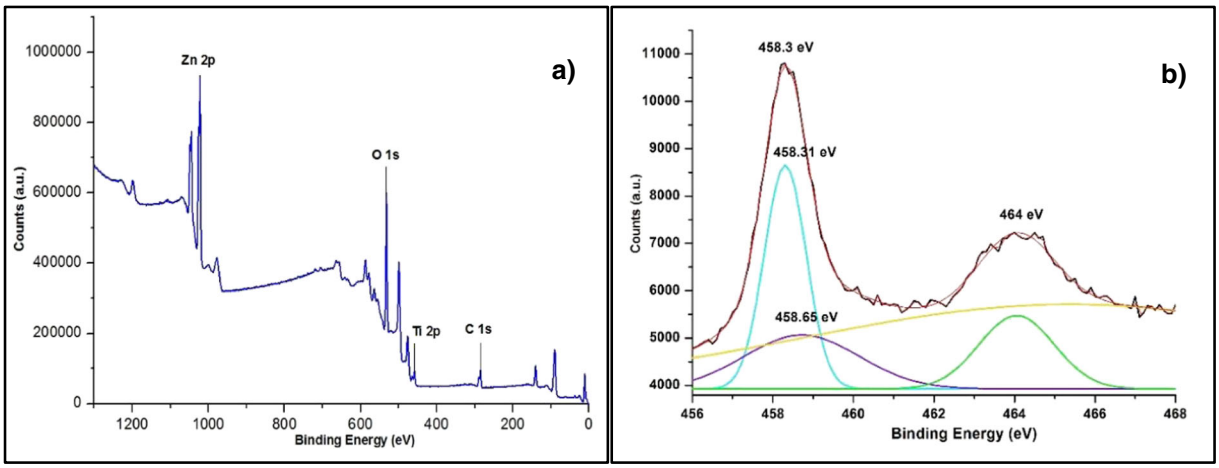

Fig. 2 **a** Full XPS survey scan and **b** Ti 2p spectrum of Zn-Ti LDH

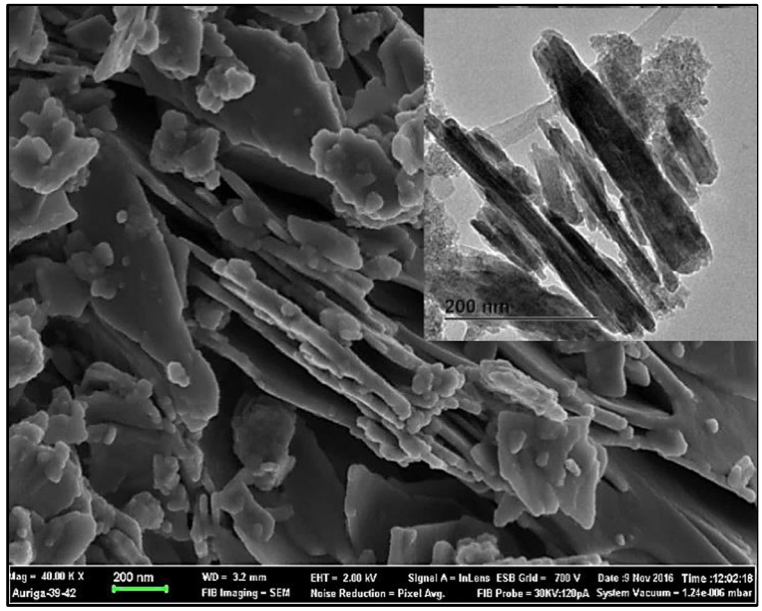

Fig. 3 SEM and TEM micrographs for Zn-Ti LDH

contrary to what was expected. Over the past few years, scientists have been of the understanding that inorganic UV filters provide protection by reflecting UVR which interacts with the nanoparticles (Kollias 1999). However, the results obtained in this study suggest that ZnO and TiO_2 have very low reflectance capabilities whereas Zn-Ti LDH exhibits heightened levels of reflectance in the UV region (both UVA and UVB).

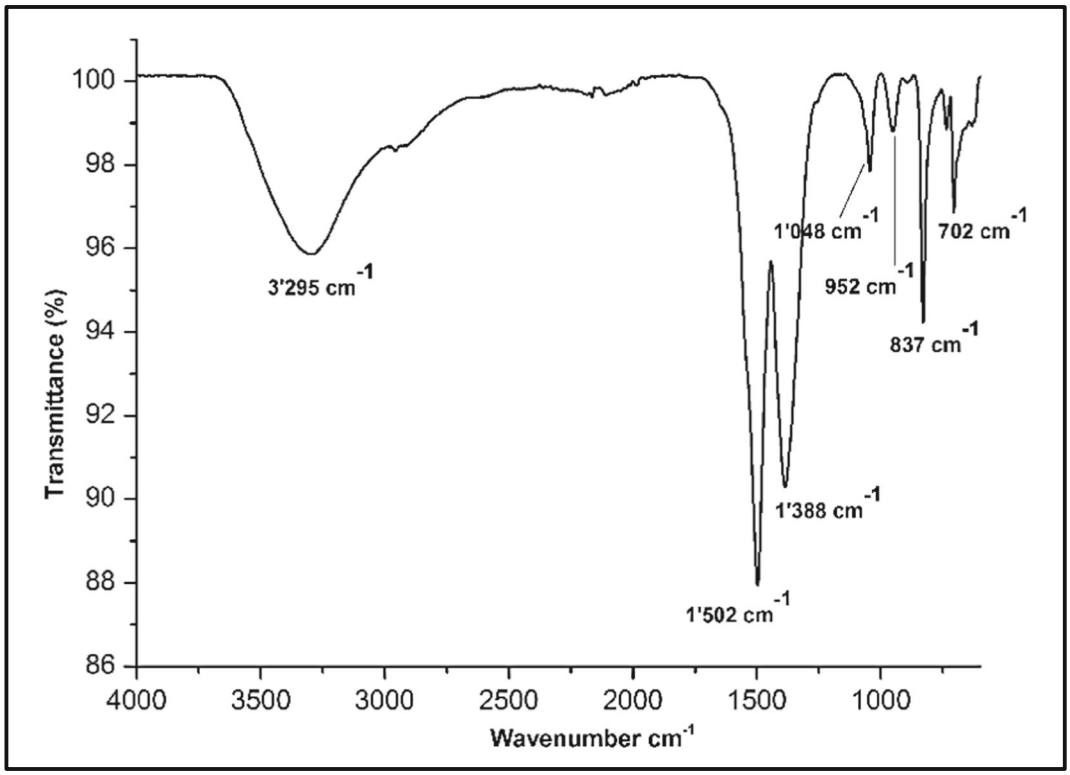

Fig. 4 FTIR spectrum of Zn-Ti LDH

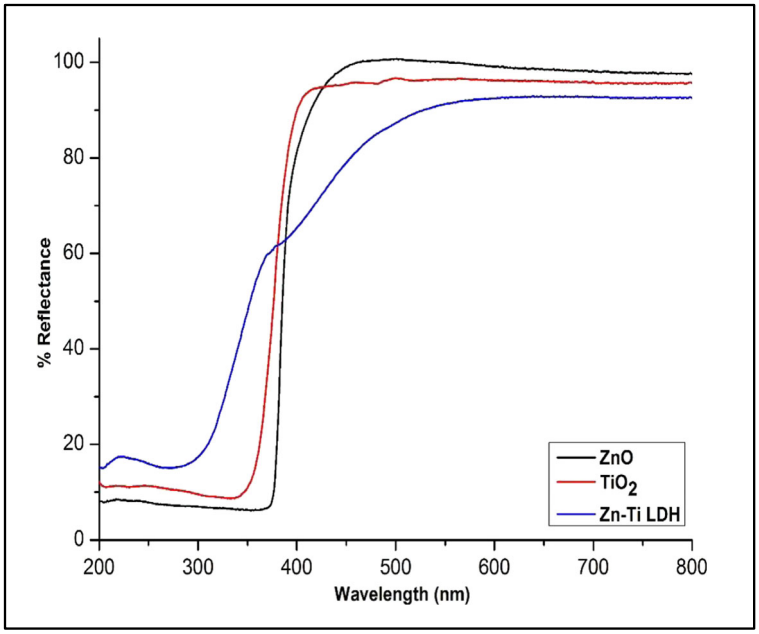

Fig. 5 Diffuse reflectance spectra of the synthesized Zn-Ti LDH and reference samples (ZnO and TiO_2)

Kubelka-Munk(K-M) equation,

$$F(R) = \left(\frac{(1-R)^2}{2R}\right) \text{.....3}$$

where R is the value of the absolute reflectance of the samples was used to convert the reflectance values obtained from the DRUV-Vis into the equivalent absorption coefficient (α) which is proportional to F(R) (Khan et al. 2013). The plot thus obtained is merely the absorbance of the material as a function of wavelength (refer Fig. 6). The direct correlation between Figs. 5 and 6 indicates that the reflectance and absorbance capabilities of the materials are inversely proportional to each other.

From Fig. 6, it is apparent that of the studied materials, ZnO has the highest UV absorbance capabilities followed by TiO_2. Attention must be drawn to the fact that the Zn-Ti LDH exhibits the lowest absorbance within the UV region relative to the references. These results coincide with reports by Cole et al. (2016) and

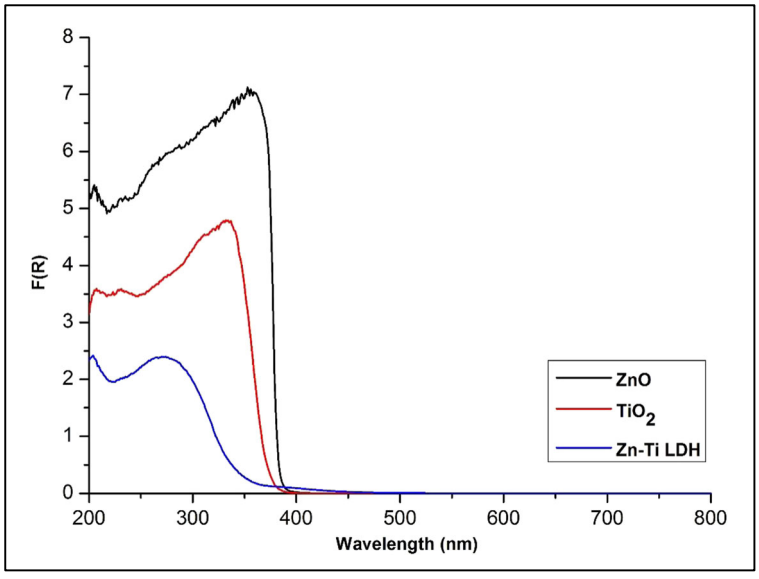

Fig. 6 Kubelka-Munk plots for Zn-Ti LDH and the reference samples (ZnO and TiO_2)

Kollias (1999) indicating that inorganic filters such as TiO_2 and ZnO exhibit UV absorptive properties rather than the previous notion that their mode of action was to solely reflect light (Serpone et al. 2007; Manaia et al. 2013; Reinosa et al. 2016). Since Zn-Ti LDH is a material of low UV absorption capability, its higher surface area compared to ZnO and TiO_2 could provide higher number of particles with multiple angles for the effective diffuse reflection of UVR.

The use of the Kubelka-Munk function F (R) (which is assumed to be proportional of absorption coefficient α) in Tauc equation,

$$(h\nu\alpha)^{1/n} = \mathrm{A}\left(h\nu - E_g\right).....4 \quad (3)$$

(where h is the Plank's constant, ν is the frequency of light, E_g is the band gap, and n is the order of electronic transition, the value of which is ½, 3/2, 2, and 3 for direct allowed, direct forbidden, direct forbidden, and indirect forbidden transitions), allowed the determination of the band gap of the materials. Tauc plots of $[F(R)h\nu]^{1/n}$ versus $h\nu$ and the intercept of the linear portion provide information regarding E_g. The electronic transition from the valence band to the conduction band for the synthesized Zn-Ti LDH is taken as a direct allowed direct transition, which is the same as ZnO ($n = 1/2$). However, for TiO_2, the transition is a forbidden direct transition where $n = 2$. For the Zn-Ti LDHs, the transition is from the 2p orbital of the oxygen to the metals 4s or 4p levels. The transition does not involve the d-orbitals as Zn is a d10 metal, and thus, its corresponding ion Zn^{2+} has no empty d-orbitals available for bonding interactions (Ahmed et al. 2012a, b).

Figure 7a–c show the Tauc plots for the reference samples as well as the synthesized Zn-Ti LDH. The band gap for the references TiO_2 and ZnO were 3.23 eV and 3.27 eV respectively. These values correlate well with reported values (Smijs and Pavel 2011). However, Fig. 7c shows the band gap for Zn-Ti LDH as 3.72 eV, which is shifted to higher energy value, a red shift, in comparison to ZnO and TiO_2. This shift is attributed to the incorporation of Zn and Ti in a hierarchal structure (Ali and Muhammad 2012). This broadening of the band gap predicted lower photocatalytic properties for the Zn-Ti LDH.

Methylene blue adsorption studies

There are several reports in literature wherein LDHs have been used nanosized adsorbent for the removal of organic pollutants such as dyes from waste water (Zubair et al. 2017; Ayawei et al. 2015). In many instances, the LDHs have been modified either by calcination or by the addition of a surfactant such as sodium dodecyl sulfate, which ultimately improves the adsorption capabilities of the LDHs (Li and Duan 2006). Given these reports, it is necessary to determine the rate of adsorption of MB onto the material surface so as not to misinterpret it as the degradation of MB under UVR at a later stage (Starukh et al. 2016). The affinity of the different sample surfaces towards MB was studied through adsorption experiments and the results are presented in Table 1.

From Table 1, it is apparent that the adsorption of MB on the LDH surface is negligible when analyzing the photodegradation of MB. However, ZnO and TiO_2 show relatively higher levels of MB adsorption to that of Zn-Ti LDH. MB is a positively charged, heterocyclic aromatic dye which may be degraded further into a monomer and dimer over time. LDHs typically exhibit good anionic exchange capability which allows for the intercalation and sorption of negatively charged species onto the interlayer spaces rather than to the positively charged surface. Therefore, the decreased adsorption capability in this case may be attributed to the net positive surface charge of Zn-Ti LDH due to the presence of Ti^{4+} within the structure which prevents the positively charged ions of MB from adsorbing on to its surface. This electrostatic interaction between the dye anions and the surface is the rate determining step in the entire adsorption process (Starukh et al. 2016).

Photodegradation of methylene blue

Several reports indicate that ZnO and TiO_2 are great photocatalysts and are prone to generate reactive oxygen species (ROS) when they encounter UVR ultimately rendering them relatively unsafe for use in cosmetic applications (Smijs and Pavel 2011). To determine the capability of the synthesized LDHs to generate ROS, the photodegradation studies of MB was employed.

Figure 8 shows the extent of MB photodegradation obtained for the synthesized LDH, ZnO, and TiO_2 during their irradiation for a total of 4 h under UVB (254 nm) and UVA (365 nm). The largest decrease in absorbance was observed for TiO_2, while the Zn-Ti LDH appeared to be the least photocatalytically active sample, with the smallest decrease in absorbance under both UVA and UVB. From Fig. 8, it is apparent that ZnO and TiO_2 degrade MB at a faster rate than Zn-Ti LDH through the generation of free radicals. During the reaction, the solutions containing these references changed from an initial deep blue color to a

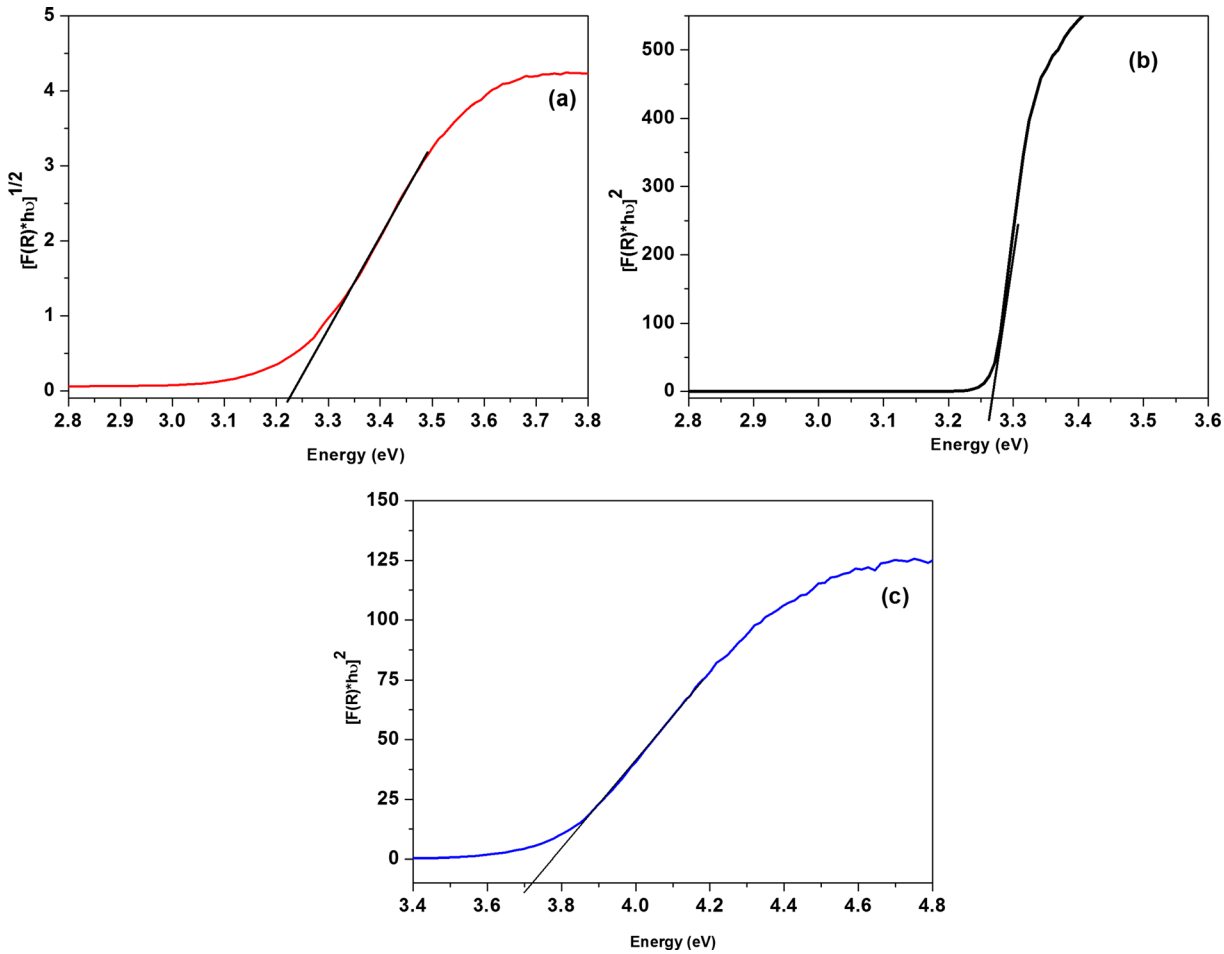

Fig. 7 Tauc plots showing the band gap for **a** TiO_2, **b** ZnO, and **c** Zn-Ti LDH

murky, white solution. It is interesting to note that despite the energy of the UVR exceeding the band gap of the Zn-Ti LDH, the photocatalytic activity remains minimal. For ZnO and TiO_2, the biggest difference in absorbance readings occurred between 0 and 1 h. Hence, the highest rate of photodegradation occurred within the first hour of UVR irradiation. In comparison, the Zn-Ti LDH exhibited a gradual but nominal decrease in MB absorbance.

Table 2 compares the percentage of MB photodegradation during the UVR irradiation for different samples. It is observed that Zn-Ti LDH exhibited relatively low levels of photocatalytic activity under both wavelengths, with the lowest levels existing under 365 nm which could be attributed to its higher bandgap that requires very high energy for the electron excitation from valence to the conduction band. In comparison to ZnO and TiO_2 which exhibited maximum degradation levels at 53.8% and 86%, respectively, the Zn-Ti LDH is considered to be mildly photocatalytic at 254 nm. ZnO being a semiconductor with direct allowed transitions has high

Table 1 Methylene blue adsorption capabilities of the various samples

Sample	C_0	C	C/C_0	(C_0-C)	q_e
Zn-Ti LDH	0.286100	0.273438	0.955743	0.012662	0.158275
ZnO	0.700862	0.514621	0.734269	0.186241	2.328013
TiO_2	0.886841	0.630672	0.711144	0.256169	3.202113

*[sorbent] = 0.08 g/L and [MB] = 5 ppm

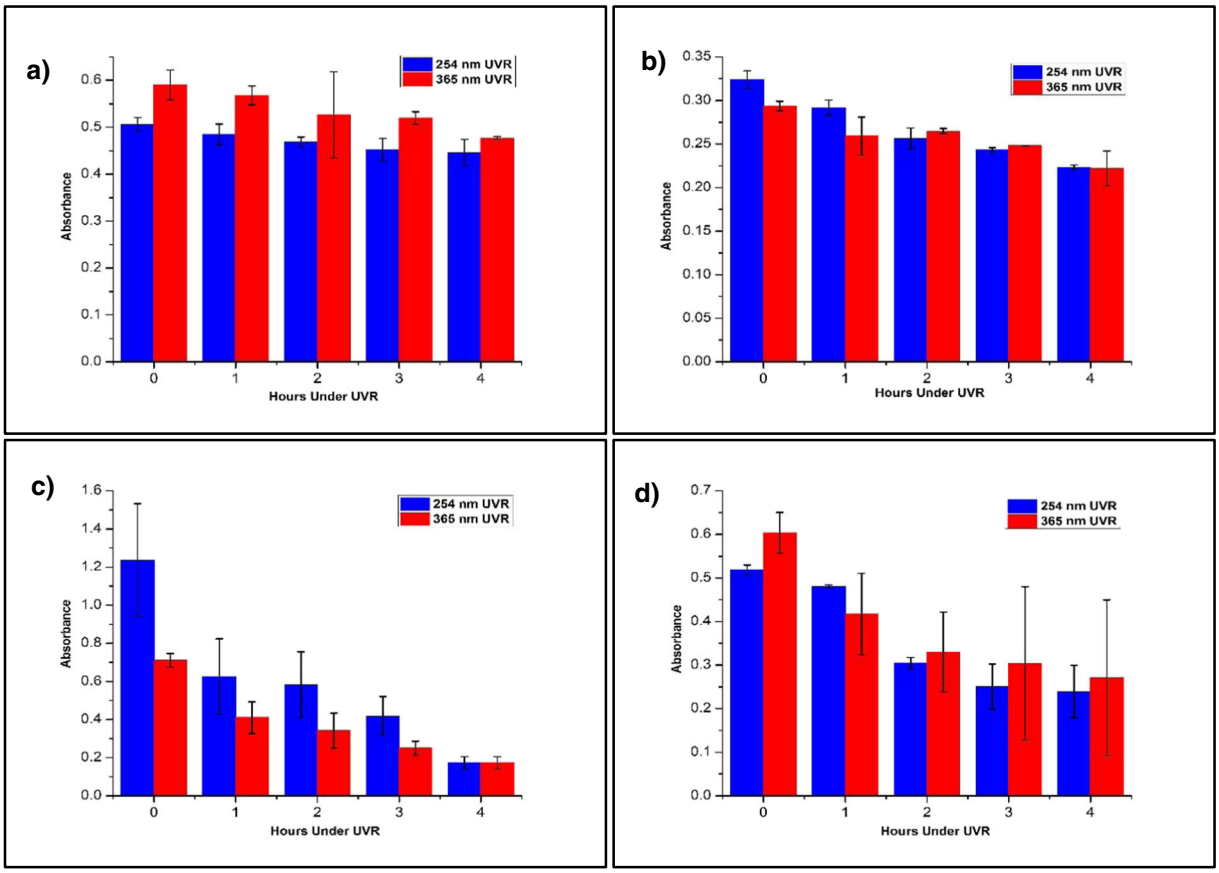

Fig. 8 Extent of MB photodegradation under 254 nm and 365 nm UVR for **a** blank (no sorbent), **b** Zn-Ti LDH, **c** TiO_2, and **d** ZnO

optical absorption coefficients and hence higher UV absorption than that of TiO_2 with indirect allowed transitions. However, for the same reason, TiO_2 exhibits a longer life of photoexcited electrons and holes which reduces the probability of electron-hole recombination, whereas the direct transitions of photogenerated electrons from the conduction band to valence band increases the chance of recombination in ZnO (Zhang et al. 2014). This explains the higher photocatalytic activity of TiO_2 although ZnO showed similar bandgap value to TiO_2. It is also noteworthy that the solution containing only MB without any sample (blank) also showed MB photodegradation.

Table 2 Percentage of methylene blue photodegradation under different wavelengths

Sample	% MB degradation ($\lambda = 254$ nm) (%)	% MB degradation ($\lambda = 365$ nm) (%)
Zn-Ti LDH	31.1 ± 0.003	24.5 ± 0.020
TiO_2	86 ± 0.032	75.6 ± 0.032
ZnO	53.8 ± 0.060	55.1 ± 0.178
Blank (no sample)	19.18 ± 0.028	11.97 ± 0.003

The low photocatalytic activity of Zn-Ti LDH may be attributed to the incorporation of Ti^{4+} within the LDH structure, which might have acted as a cationic dopant. This could result in the formation of localized *d*-states within the band gap that can function as recombination centers for photoexcited electrons and holes. Recombination centers enhance the switching of electrons and facilitate the movement of electrons and holes between energy levels which may allow their recombination, ultimately inhibiting the formation of reactive oxygen species (ROS) such as hydroxyl radicals and superoxide anion radicals (Ali and Muhammad 2012). The presence of such recombination centers could account for the reduction of photocatalytic activity observed for the Zn-Ti LDH. Given its band gap of 3.72 eV, and its overall low percentages of MB photodegradation, it is evident that Zn-Ti LDH as a cosmetic ingredient poses the lowest threat with regard to the production of ROS on UVR exposure which ensures skin safety for the consumer.

This makes it an ideal candidate for a wide range of applications within the cosmetic field particularly sunscreen formulations.

Sun protection factor

The in vitro evaluation of UVB protection was first proposed in 1989 by Diffey (Diffey and Robson 1989) and since then, there are several methods to determine the SPF value within this region. The use of Mansur's equation (Mansur et al. 1986) is beneficial wherein there are inorganic and organic components which allows for the SPF determination using spectrometry only rather than conventional in vitro methods which may have compromised results. Using the UV transmittance data obtained for the Zn-Ti LDH, the SPF was determined using Mansur's equation and the normalized product functions and calculations are shown in Table 3.

The SPF value calculated as per Mansur's equation for the Zn-Ti LDH was 17.9. Ng'etich et al. (2014) determined the SPF offered by natural clay samples collected from different parts of Kenya using an in vitro spectrometric method. The SPF values measured for most of the clays were below five with an exception of two samples showing higher SPF values of 40.98 and 27.05. In another study, Madikizela et al. (2017) reported an SPF of 1.18 for a natural clay mineral using Mansur's method. In our study, SPF of 17.9 is closely related to the attenuation of UVB radiation and provides a clear indication of the ability of this material to provide shielding capacity for UV radiation between 290 and 320 nm. The assessment of skin compatibility of Zn-Ti LDH, optimization, and sun protection performance evaluation (in vivo) of Zn-Ti LDH-based sunscreen formulations are in progress.

Table 3 Normalized product function calculations as per Mansur's equation

Wavelength (nm)	EE × *I* (normalized)	Abs. (λ)	EE (λ) × *I* (λ) × Abs. (λ)
290	0.015	2.22	0.0333
295	0.0817	2.11	0.173
300	0.2874	1.97	0.567
305	0.3278	1.79	0.589
310	0.1864	1.59	0.297
315	0.0839	1.36	0.114
320	0.018	1.11	0.0201

Conclusions

The synthesis of a Zn-Ti LDH using hydrothermal method was carried out during this study and the material was characterized accordingly. The photochemical properties of the synthesized materials were evaluated and compared to known cosmetic references: nano-ZnO and nano-TiO_2. DRUV-Vis revealed the reflectance capabilities of the materials, and the results showed that Zn-Ti LDH exhibited greater diffuse reflectance in the UV region in comparison to ZnO and TiO_2. Furthermore, the broader band gap of the Zn-Ti LDH (3.72 eV) resulted in lower UVA and UVB absorption and hence a significantly lower photocatalytic activity under UVR. This was ascribed to the formation of recombination centers which prevented formation of reactive oxygen species. A preliminary investigation of the SPF was conducted and the Zn-Ti LDH exhibited an SPF value of approximately 18 which clearly indicates its ability to effectively shield UVR and its high prospects in topical sunscreen formulations.

Acknowledgements We would like to acknowledge the help of Ms. Louise Mostert at the National Metrology Institute of South Africa (NMISA) for her XPS expertise. We acknowledge the assistance of Ms. Dina Oosthuizen for the DRUV-Vis analyses done at the University of Free State.

Funding information This work was supported by the National Research Foundation (Grant No. 100849) and Council for Scientific and Industrial Research (National Centre for Nanostructured Materials), Project HGER70P.

Compliance with ethical standards

Conflict of interest The authors declare that they have no conflict of interest.

References

Ahmed AAA, Talib ZA, Bin Hussein MZ, Zakaria A (2012a) Zn-Al layered double hydroxide prepared at different molar ratios: preparation, characterization, optical and dielectric properties. J Solid State Chem 191:271–278. https://doi.org/10.1016/j.jssc.2012.03.013

Ahmed AAA, Talib ZA, bin Hussein MZ (2012b) Thermal, optical and dielectric properties of Zn-Al layered double hydroxide. Appl Clay Sci 56:68–76. https://doi.org/10.1016/j.clay.2011.11.024

Ali A, Muhammad A (2012) Doped metal oxide (ZnO) and photocatalysis: a review. J Pakistan Inst Chem Eng 40:11–19. https://doi.org/10.5539/apr.v4n3p75

Ayawei N, Ekubo AT, Wankasi D, Dikio ED (2015) Synthesis and application of layered double hydroxide for the removal of copper in wastewater. Int J Chem 7:122. https://doi.org/10.5539/ijc.v7n1p122

Cole C, Shyr T, Ou-Yang H (2016) Metal oxide sunscreens protect skin by absorption, not by reflection or scattering. Photodermatol Photoimmunol Photomed 32:5–10. https://doi.org/10.1111/phpp.12214

Cursino ACT, da Silva Lisboa F, dos Santos Pyrrho A, de Sousa VP, Wypych F (2013) Layered double hydroxides intercalated with anionic surfactants/benzophenone as potential materials for sunscreens. J Colloid Interface Sci 397:88–95. https://doi.org/10.1016/j.jcis.2013.01.059

Diffey BL, Robson J (1989) A new substrate to measure sunscreen protection factor throughout the ultraviolet spectrum. J Soc Cosmetic Chem 40:127–133

Fajzulin I, Zhu X, Möller M (2015) Nanoparticulate inorganic UV absorbers: a review. J Coat Technol Res 12:617–632. https://doi.org/10.1007/s11998-015-9683-2

Khan MM, Ansari SA, Amal MI, Lee J, Cho MH (2013) Highly visible light active Ag@TiO<inf>2</inf> nanocomposites synthesized using an electrochemically active biofilm: a novel biogenic approach. Nanoscale 5:4427–4435. https://doi.org/10.1039/c3nr00613a

Kollias N (1999) The absorption properties of "physical" sunscreens. Arch Dermatol 135:209–210. https://doi.org/10.1001/archderm.135.2.209-a

Li F, Duan X (2006) Applications of Layered double hydroxides. Struct Bond 119:193–223. https://doi.org/10.1007/430_007

Li Y, Tang L, Ma X, Wang X, Zhou W, Bai D (2017) Synthesis and characterization of Zn-Ti layered double hydroxide intercalated with cinnamic acid for cosmetic application. J Phys Chem Solids 107:62–67. https://doi.org/10.1016/j.jpcs.2017.02.018

Madikizela LM, Nkwentsha N, Mlunguza NY, Mdluli PS (2017) Physicochemical characterization and in vitro evaluation of the sun protection factor of cosmetic products made from natural clay material S Afr J Chem 70:113–119. https://doi.org/10.17159/0379-4350/2017/v70a016

Manaia EB, Kaminski RCK, Corrêa MA, Chiavacci LA (2013) Inorganic UV filters. Braz J Pharm Sci 49:201–209. https://doi.org/10.1590/S1984-82502013000200002

Mansur JS, Breder MN, Mansur MCAR (1986) Determination of sun protection factor by spectrophotometric methods. An Bras Dermatol 61:121–124

Ng'etich WK, Mwangi EM, Kiptoo J, Digo CA, Ombito JO (2014) *In vitro* determination of sun protection factor on clays used for cosmetic purposes in Kenya. Chem Mater Res 6:25–30

Perioli L, Ambrogi V, Bertini B, Ricci M, Nocchetti M, Latterini L, Rossi C (2006) Anionic clays for sunscreen agent safe use: photoprotection, photostability and prevention of their skin penetration. Eur J Pharm Biopharm 62:185–193. https://doi.org/10.1016/j.ejpb.2005.08.001

Reinosa JJ, Leret P, Álvarez-Docio CM, Campo A, Fernándeza JF (2016) Enhancement of UV absorption behavior in ZnO-TiO_2 composites. Bol la Soc Esp Ceram y Vidr 55:55–62. https://doi.org/10.1016/j.bsecv.2016.01.004

Saber O, Tagaya H (2003) New layered double hydroxide, Zn-Ti LDH: preparation and intercalation reactions. J Incl Phenom 45:109–116

Seftel EM, Popovici E, Mertens M, van Tendeloo G, Cool P, Vansant EF (2008) The influence of the cationic ratio on the incorporation of Ti^{4+}in the brucite-like sheets of layered double hydroxides. Microporous Mesoporous Mater 111:12–17. https://doi.org/10.1016/j.micromeso.2007.07.008

Seftel EM, Niarchos M, Vordos N, Nolan JW, Mertens M, Mitropoulos AC, Vansant EF, Cool P (2015) LDH and TiO_2/LDH-type nanocomposite systems: a systematic study on structural characteristics. Microporous Mesoporous Mater 203:208–215. https://doi.org/10.1016/j.micromeso.2014.10.029

Serpone N, Dondi D, Albini A (2007) Inorganic and organic UV filters: their role and efficacy in sunscreens and suncare products. Inorg Chim Acta 360:794–802. https://doi.org/10.1016/j.ica.2005.12.057

Shao M, Han J, Wei M, Evans DG, Duan X (2011) The synthesis of hierarchical Zn-Ti layered double hydroxide for efficient visible-light photocatalysis. Chem Eng J 168:519–524. https://doi.org/10.1016/j.cej.2011.01.016

Silva CG, Bouizi Y, Fornés V, Garcia H (2009) Layered double hydroxides as highly efficient photocatalysts for visible light oxygen generation from water. J Am Chem Soc 131:13833–13839. https://doi.org/10.1021/ja905467v

Smijs TG, Pavel S (2011) Titanium dioxide and zinc oxide nanoparticles in sunscreens: focus on their safety and effectiveness. Nanotechnol Sci Appl 4:95–112. https://doi.org/10.2147/NSA.S19419

Starukh G, Rozovik O, Oranska O (2016) Organo/Zn-Al LDH nanocomposites for cationic dye removal from aqueous media. Nanoscale Res Lett 11. https://doi.org/10.1186/s11671-016-1402-0

Tshabalala ZP, Shingange K, Cummings FR, Ntwaeaborwa OM, Mhlongo GH, Motaung DE (2017a) Ultra-sensitive and selective NH_3 room temperature gas sensing induced by manganese-doped titanium dioxide nanoparticles. J Colloid Interface Sci 504:371–386. https://doi.org/10.1016/j.jcis.2017.05.061

Tshabalala ZP, Shingange K, Dhonge BP, Ntwaeaborwa OM, Mhlongo GH, Motaung DE (2017b) Fabrication of ultra-high sensitive and selective CH4room temperature gas sensing of TiO_2 nanorods: detailed study on the annealing temperature. Sensors Actuators B Chem 238:402–419. https://doi.org/10.1016/j.snb.2016.07.023

Xu ZP, Braterman PS (2010) Synthesis, structure and morphology of organic layered double hydroxide (LDH) hybrids: comparison between aliphatic anions and their oxygenated analogs. Appl Clay Sci 48:235–242. https://doi.org/10.1016/j.clay.2009.11.009

Zhang X, Qin J, Xue Y, Yu P, Zhang B, Wang L, Liu R (2014) Effect of aspect ratio and surface defects on the photocatalytic activity of ZnO nanorods. Sci Rep 4:4–11. https://doi.org/10.1038/srep04596

Zubair M, Daud M, McKay G, Shehzad F, Al-Harthi MA (2017) Recent progress in layered double hydroxides (LDH)-containing hybrids as adsorbents for water remediation. Appl Clay Sci 143:279–292. https://doi.org/10.1016/j.clay.2017.04.002